IEEE Access
Multidisciplinary | Rapid Review | Open Access Journal

Received May 10, 2018, accepted June 25, 2018, date of publication July 16, 2018, date of current version August 7, 2018.

Digital Object Identifier 10.1109/ACCESS.2018.2853194

Fast Super-Resolution Ultrasound Imaging With Compressed Sensing Reconstruction Method and Single Plane Wave Transmission

YUEXIA SHU[1], CHANGPENG HAN[2], MINGLEI LV[1], AND XIN LIU[1], (Member, IEEE)

[1]School of Communication and Information Engineering, Shanghai University, Shanghai 200444, China
[2]Department of Coloproctology, Yueyang Hospital of Integrated Traditional Chinese and Western Medicine, Shanghai University of Traditional Chinese Medicine, Shanghai 200437, China

Corresponding author: Xin Liu (xinliu.c@gmail.com)

This work was supported by the National Natural Science Foundation of China under Grant 81371604, Grant 61571281, and Grant 81403399.

ABSTRACT Super-resolution ultrasound (SR-US) imaging technique breaks the diffraction limit and can image microvascular structure. However, the temporal resolution of SR-US is limited because a long data acquisition time is required to accumulate enough microbubbles. To overcome this limitation, in this paper, we proposed a new SR-US method based on compressed sensing (CS), which is used to identify the highly overlapped microbubbles in each frame. To further speed up the data acquisition of SR-US, here, U.S. data was generated by single plane wave (SPW) transmission. To evaluate the performance of the proposed technique (CS reconstruction method combined with SPW transmission, termed as CSRM-SPW), a series of numerical simulation was performed. Especially, considering that SPW has a relatively low spatial resolution, it may affect the obtained SR-US imaging performance. We compare the effect of synthetic transmit aperture (STA) and SPW on SR-US. The results indicate the overlapped microbubbles can be identified by the CSRM method when compared with the traditional localization method (e.g., Gaussian fitting method). In addition, whatever STA or SPW images are used as the input data of CS reconstruction, the localization accuracy of SR-US obtained by the CSRM method is similar. Further, by using the CSRM combined with SPW technique, the vascular network can be accurately resolved, even if the high-density microbubbles existed in each frame. As a result, the proposed CSRM-SPW technique is suitable for fast SR-US imaging.

INDEX TERMS Biomedical imaging, ultrasound imaging, microbubbles, super-resolution ultrasound, compressed sensing.

I. INTRODUCTION

Ultrasound (US) is a widely used clinical imaging modality, which provides penetration depth in tissues tens of centimeters [1]. However, the spatial resolution of US is limited due to the diffraction limit. When using the shorter wavelength, the spatial resolution can be increased, but it will result in a lower penetration depth.

Inspired by the super-resolution technology in optical microscopy, e.g., stochastic optical reconstruction microscopy (STORM) [2] or photoactivated localization microscopy (PALM) [3], with the aid of the microbubbles, the super-resolution ultrasound (SR-US) techniques have been proposed [4]–[9]. In short, by locating the isolated microbubbles in each US frame and then superimposing the identified positions of microbubbles from all frames into a image, a final SR-US image is obtained. Compared with the traditional US modality, SR-US overcomes the diffraction limit, which provides a new method for super-resolution imaging of microvascular structure [4]–[9].

Despite these achievements, the temporal resolution of SR-US is limited. The main problem is that to implement SR-US imaging, the microbubbles in each US frame need to be sparse enough that the position of each microbubble can be accurately identified [4], [5]. As a result, it need take a long time to collecting data for accumulating enough microbubbles, which greatly increases its temporal resolution. To reduce the imaging time, a feasible strategy is by using US data with the higher density microbubbles in

each frame. However, the high-density microbubbles may overlapp. The current single-emitter localization methods (e.g., the Gaussian fitting method) are difficulty in accurately resolving these overlapped microbubbles.

To address this problem, in super-resolution optical microscopy, a method based on compressed sensing (CS) theory has been proposed [10]–[12]. By applying CS to STORM imaging model, Zhu *et al.* [10] demonstrate the capability of CS method in super-resolution optical imaging, where the higher density of emitters can be localized compared with the traditional localization methods. Based on the above consideration, in this paper, the reconstruction method based on CS (termed as CSRM) is introduced to SR-US imaging model to identify highly overlapped microbubbles and improve the temporal resolution of SR-US. On the other hand, to further speed up the data acquisition of SR-US, in this paper, US images are acquired by single plane wave (SPW) transmission. By using unfocussed beams to illuminate the whole imaging region at only one emission, SPW imaging technique can achieve ultrafast US imaging [13], [14]. But, the spatial resolution of SPW is relatively low, which may affect the obtained imaging performance of SR-US. Considering that the synthetic transmit aperture (STA) can obtain a highest possible spatial resolution, compared with other US imaging modalities [15], [16], in this work, we especially investigate the effect of STA (the high-resolution US) and SPW (the low-resolution US) on the imaging performance of SR-US. It is important for evaluating the feasibility of the proposed technique (CS reconstruction method combined with SPW transmission, termed as CSRM-SPW) in fast SR-US imaging study.

To evaluate the performance of the CSRM-SPW technique, in this paper, we designed three types of numerical simulation experiments. Firstly, a phantom, including the overlapped point scatterers, was generated. Based on the phantom model, we mainly investigate the capability of the CSRM method in identifying the highly overlapped microbubbles. Secondly, we evaluate the effect of SPW and STA on SR-US imaging performance implemented by the CSRM method. In the case, US data from a phantom model including six point scatterers with variable signal-to-noise ratios (SNRs) were generated and used. Finally, a flowing vasculature model was generated, where the high density microbubbles were filled in the vasculature. The flowing vasculature model was used to evaluate the capability of the CSRM-SPW technique in imaging microbubbles flowing through vascular network. The results indicate that when using the proposed CSRM method, the overlapped microbubbles can be accurately resolved, compared with the traditional localization methods (e.g., Gaussian fitting method). In addition, when using the CSRM method, the localization accuracy of SR-US is similar, whatever STA or SPW images are used to reconstruct the super-resolution results. Further, the blood vessel network can be accurately resolved by the proposed CSRM-SPW technique, even through the high density microbubbles existed in each US frame. As a result, the CSRM-SPW technique is suited for fast SR-US imaging because: 1) the highly overlapped microbubbles in each frame can be accurately identified, which can reduce the number of frames used to implement the SR-US imaging; 2) the use of SPW transmission technique further speeds up the data acquisition of SR-US.

The paper is organized as follows. In Section II, the methods, including in STA and SPW imaging techniques, and CS localization method are described. In Section III, the simulation materials are shown. Section IV describes the experimental results. Finally, we discuss the results and draw conclusions in Section V.

II. METHODS

A. SPW AND STA IMAGING

In STA imaging, a single element in transmitting aperture is excited for transmitting a US wave. The echo signals are received by all elements. For each transmission, the dynamic receive focusing (DRF) is performed, and a low-resolution image is obtained. The above procedure is repeated for each element in transducer aperture. Finally, a high-resolution image is generated by summing all low-resolution images (see Fig. 1(a)) [15], [16].

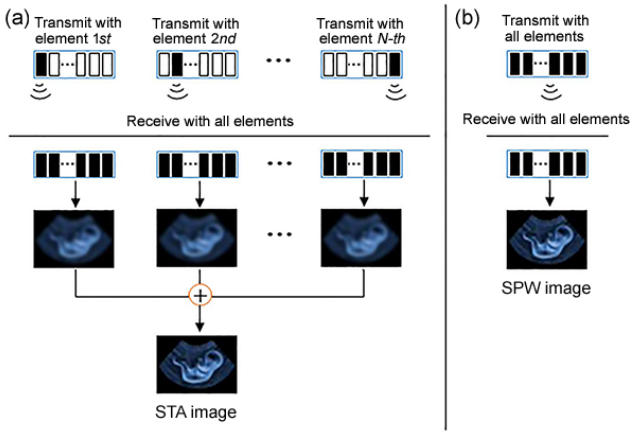

FIGURE 1. The schematic of the SPW and STA imaging. (a) In STA imaging, a single element in transmitting aperture is excited and all elements in receiving aperture are used to collect the echo signals. This data is used to generate a low-resolution image. This procedure is repeated for each element in transducer aperture. Finally, a high-resolution image is obtained by summing all low-resolution images. (b) In SPW imaging, the full image region is excited by a single unforced plane wave generated by all elements in transmitting aperture, and echo signals are acquired by all elements in receiving aperture. By beamforming the echo data, a US image is generated.

STA can implement dynamic focusing both on transmit and receive channel. As a result, STA can obtain a highest possible spatial resolution, compared with other US imaging modalities [13], [14]. However, the imaging time of STA is high since the element need to be activated in turn in whole imaging processes.

Comparably, in SPW imaging processes, the full image region is excited by a single unforced plane wave generated by all elements in transmitting aperture, and the echo

signals are acquired by all elements in receiving aperture (see Fig. 1(b)). Sequentially, the radio-frequency data is beamformed by DRF method and a US image is generated [14]. As a result, in SPW imaging, one plane wave illumination and massive parallel receive beamforming can result in ultrafast US imaging. Hence, it is suitable for imaging fast events within the sample. But, the spatial resolution of SPW is relatively low due to the use of unfocused beams on the transmit channel.

B. THE SUPER-RESOLUTION IMAGING METHOD BASED ON CS

Based on the current localization methods, to implement SR-US imaging, it is necessary to sample US images with low microbubble density, leading to the low temporal resolution. To overcome the limitation, a strategy is by using US data with the high-density microbubbles in each frame. However, the current localization methods are difficulty in accurately resolving the localizations of these high-density microbubbles.

Based on compressed sensing (CS) theory, if the original signal $x \in R^n$ is sparse or compressible, it can be recovered from m measurement data, with $m \ll n$ [17]. Due to the advantage, a method based on CS has been proposed and successfully applied to super-resolution localization microscopy to identify the high-density emitters [10]. For SR-US imaging, the sparsity of signal $x \in R^n$ is true, because the underlying structure to be imaged (e.g., microvascular structure) is sparsely disturbed in each frame. Based on the above consideration, CS can also be used to locate the high density microbubbles even though they overlap in each US frame.

Referring to [10], there is a linear relationship between the acquired US image and the true microbubble locations in each frame, as follows,

$$b = \mathbf{A}x \tag{1}$$

where $b \in R^m$ is the experimentally acquired US image; $x \in R^n$ is the reconstructed SR-US image in which microbubble locations are presented. The elements in the vector x are the intensities of the microbubble, discretized on an image grid. Each grid point in x represents the brightness of a microbubble located at this point. $\mathbf{A} \in R^{m\times n}$ is a matrix, which is constructed from the point spread function (PSF) of US imaging system. The column i^{th} of $\mathbf{A}$ corresponds to the acquired US image, only when one microbubble exists in the position index i of x. The detailed information on construction of matrix can be referred in [10].

The goal of SR-US reconstruction is to obtain x from the measured b according to Eq. (1). To facilitate high-density microbubble localization, here, x is discretized on a sub-pixel grid with respect to the original pixel grid. Considering that in ultrasound imaging, x is sparse on a sufficiently high-resolution grid, it is possible to recover x from measurement b by solving the following constrained-minimization problem,

$$\text{minimize } \|x\|_1 \quad \text{subject to } \|\mathbf{A}x - b\|_2 \leq \varepsilon \tag{2}$$

where $\|x\|_1$ denotes the l_1-norm of x. In this paper, Eq. (2) is solved by a standard interior point method, similar to that used in [10]. By superimposing all the reconstructed x into one frame, a final super-resolution image can be obtained. In this paper, we do not intend to develop any new method for solving Eq. (2). Instead, we use a standard interior point method. Other sparsity-based method [18]–[21] can also be used to address the optimization problem and further improve the imaging performance of SR-US.

In this paper, SPW and STA are implemented by Field II [22], [23]. The reconstruction method is implemented in Matlab 7.3 combined with the CVX optimization package [24].

III. MATERIALS

Here, three types of numerical simulation experiments were designed to evaluate the performance of the CSRM-SPW technique.

A. CASE I. EVALUATING THE CAPABILITY OF THE CSRM-SPW TECHNIQUE IN IDENTIFYING THE OVERLAPPED MICROBUBBLES

Firstly, to evaluate the feasibility of the proposed CSRM-SPW technique in identifying the highly overlapped microbubbles, a phantom simulation was performed. Here, a cubical phantom with 20 $mm(Length) \times 40\ mm(Height) \times 10\ mm(Width)$ was created, where the different number of point scatterers (two and ten) was randomly distributed in the phantom and some of them overlapped. These point scatterers were used to simulate the microbubbles in tissues.

A linear array transducer with 128 elements was placed over the phantom, and its center frequency and sampling frequency were set to 7 MHz and 100 MHz, respectively. This phantom model was scanned by SPW transmission. The backscattered signals were collected and then beamformed. After that, a US image was generated, which was then used as the input data of the CSRM reconstruction method. To simulate the noise effect, referring to [25], the white Gaussian noises with different SNRs (i.e., 10, 20, 30, 40, and 50 dB), were added to the synthetic SPW images. All parameters of scan used in SPW are summarized in Table I.

B. CASE II. EVALUATING THE EFFECT OF STA AND SPW ON THE IMAGING PERFORMANCE OF SR-US IMPLEMENTED BY THE CSRM METHOD

Secondly, a cubical phantom, including six point scatterers, was created, which was mainly used to evaluate the effect of STA and SPW on the imaging performance of SR-US, when using the proposed CSRM method. In the phantom model, six scatterers were distributed in the depth of 25-35 mm in the phantom, where the lateral spacing of two adjacent scatterers was 3 mm, and the longitudinal spacing was 5 mm.

The phantom was scanned by STA and SPW. The backscattered signals from STA and SPW were collected and beamformed, respectively. After that, the corresponding US images were generated. All parameters of scan used in STA and SPW

TABLE 1. The parameters of scan used in the STA and SPW.

Parameter type	STA imaging	SPW imaging
Transducer array type	linear array	linear array
Element pitch	208 μm	208 μm
Element kerf	35 μm	35 μm
Element height	4.5 mm	4.5 mm
Speed of sound	1540 m/s	1540 m/s
Center frequency, f_0	7 MHz	7 MHz
Sampling frequency	100 MHz	100 MHz
Wavelength	220 μm	220 μm
Excitation pulse	Two-cycle sinusoid at f_0	Two-cycle sinusoid at f_0
Transmit/Receive apodization	Hanning	Hanning
Number of transmitting elements	1	128
Number of receiving elements	128	128
Number of emissions	128	1

are summarized in Table I. Similar to Case I, the different levels of Gaussian noise (i.e., SNR 10, 20, 30, 40, and 50 dB), were added to the synthetic STA and SPW images to simulate the noise effect on the imaging performance.

C. CASE III. EVALUATING THE PERFORMANCE OF THE CSRM-SPW TECHNIQUE IN RESOLVING VASCULAR NETWORK

Finally, a flowing vasculature model was generated. The simulation model was used to validate the super-resolution property of the CSRM-SPW in imaging microbubbles flowing through vascular network.

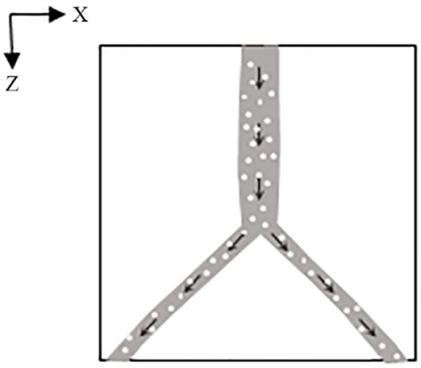

FIGURE 2. The schematic of flowing vasculature model. The gray area represents the vascular network. The microbubbles are represented by white circles. The movement directions of microbubbles are depicted by the black arrows.

As shown in Fig. 2, the vasculature model was designed to consist of a large vessel (radius ∼3 mm) and two small vessels (radius ∼1.5 mm). The length of the large vessel and two small vessels was ∼20 mm.

During the whole imaging processes, the microbubbles were assumed to move along the vascular network. Referring to [26], the movement of microbubbles is set as follows,

$$v(r) = v_0 \left[1 - \left(\frac{r}{R}\right)^2\right] \tag{3}$$

where v_0 corresponds to maximum velocity at the center of the vessel; v corresponds to the velocity; r is the distance from the microbubble to the center axis of the vessel; R is the radius of the vessel. Here, the beam-to-flow angle of the large vessel was set as 0°, the beam-to-flow angles of the two small vessels were set as −45° and 45°, and v_0 was set as 1m/s.

The bubble-filled vascular phantom was scanned by SPW transmission, implemented by a 128 element linear array. The center element was located above the vasculature model. The scan parameters for SPW were the same as those used in Case I (see Table I).

To simulate the flow of microbubbles in vasculature, a series of US data were acquired. Briefly, after each SPW transmission, the backscattered signals from all receiving elements were acquired and beamformed. A SPW image was sequentially generated. After that, a new model was created, with microbubbles moving along the vascular network (see black arrows in Fig. 2) with velocity v. For implementing the dynamic imaging, the above procedure was repeated 50 times. Finally, all 50 frame SPW images were obtained,

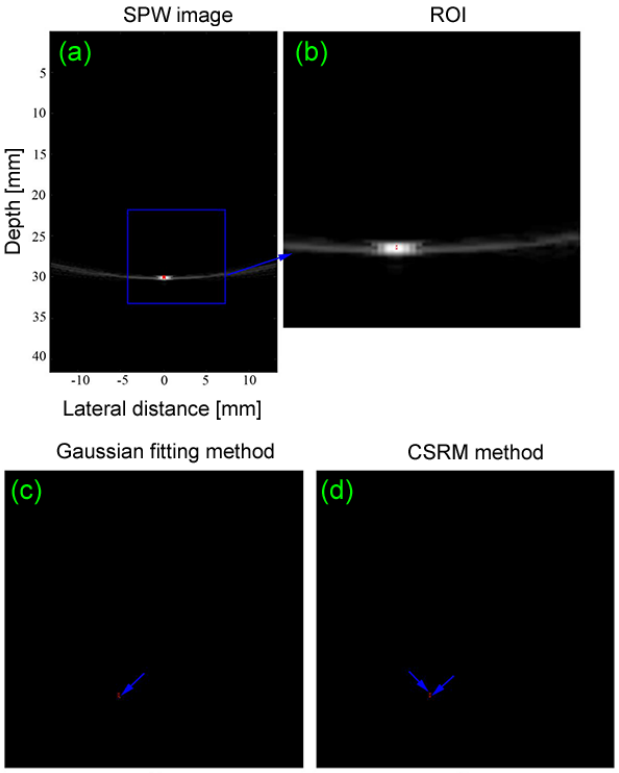

FIGURE 3. Comparison of the imaging performance of SR-US obtained by the conventional localization method (Gaussian fitting) and the proposed CSRM method. (a) The simulated SPW US image. Here, two overlapped microbubbles were included in the phantom model. (b) A zoom-in of the region of interest (ROI) outlined by the blue region in (a). (c) and (d) The SR-US results obtained by Gaussian fitting and CSRM methods. The red points depict the true locations of the two microbubbles in the phantom.

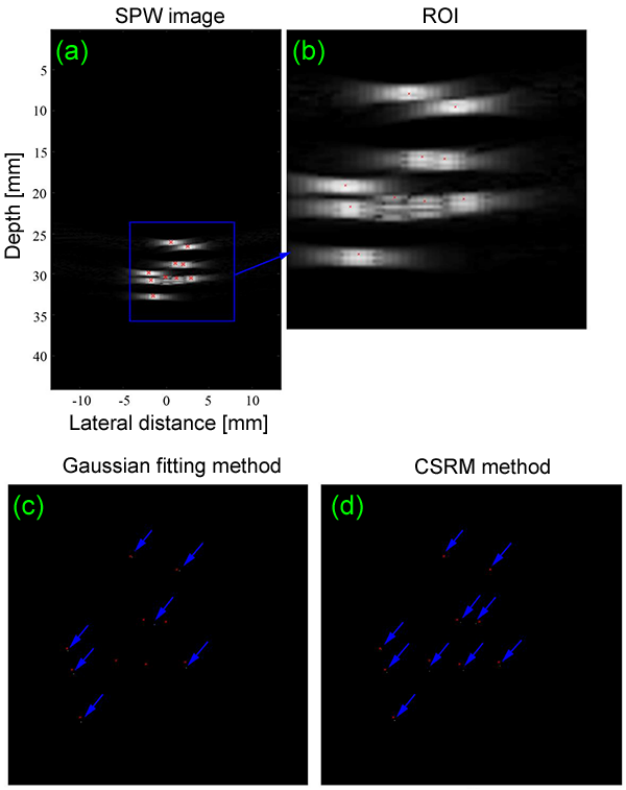

FIGURE 4. Comparison of SR-US imaging performance obtained by the Gaussian fitting and CSRM methods. (a) The simulated SPW US image, where 10 microbubbles were randomly distributed in the phantom and some of them overlapped. (b) A zoom-in of the ROI outlined by the blue region in (a). (c) and (d) The SR-US results obtained by the Gaussian fitting and CSRM methods. The red points depict the true locations of these microbubbles in the phantom.

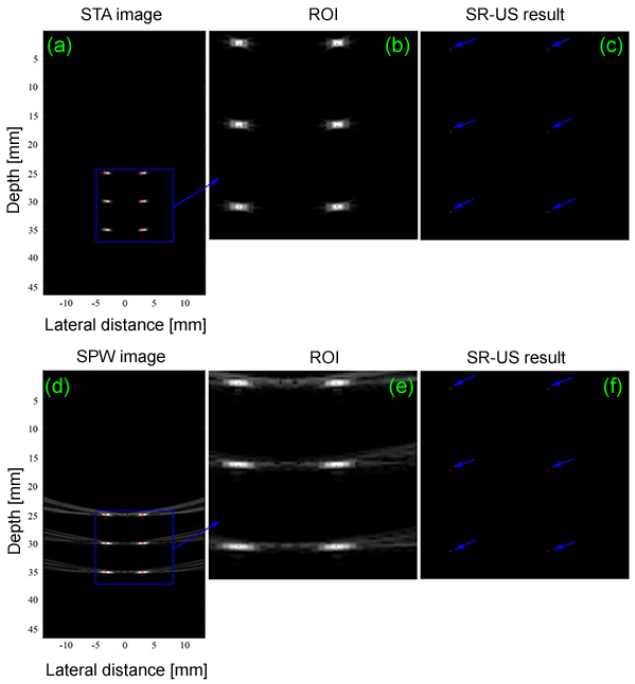

FIGURE 5. Comparison of the effect of STA and SPW on the imaging performance of SR-US implemented by the proposed CSRM method. (a) and (d) The simulated US images obtained from STA and SPW, respectively. (b) and (e) A zoom-in of the ROIs outlined by the blue regions in (a) and (d). (c) and (f) The corresponding SR-US results of (a) and (d) obtained by the CSRM method.

which were used to simulate the flow of microbubbles in vascular network.

IV. RESULTS

A. EVALUATING THE CAPABILITY OF THE CSRM-SPW TECHNIQUE IN IDENTIFYING THE OVERLAPPED MICROBUBBLES

Fig. 3 compares the imaging performance of SR-US obtained by the conventional localization method (Gaussian fitting) and CSRM method, respectively. Fig. 3(a) shows the simulated SPW US image. Here, two overlapped microbubbles were included in the phantom model, which was used to demonstrate the ability of the CSRM-SPW technique in identifying the overlapped microbubbles. Figs. 3(c) and (d) show the SR-US results obtained by the Gaussian fitting and CSRM methods, respectively. Note that in this work, for all cases, in the CSRM reconstruction processes, the grid on which x is discretized is oversampled by a factor of 8 with respect to the original grid. The results show that by using the conventional Gaussian fitting method, two overlapped microbubbles are not accurately identified, where only one microbubble can be identified (see Figs. 3(c)). In contrast, when using the proposed CSRM method, we can resolve the positions of two microbubbles, even if they overlapped (see Figs. 3(d)).

Note that in the SR-US imaging implemented by the CSRM method, the critical step involves the characterization of PSF of US imaging system. Inaccurate PSF may cause the severe decrease in SR-US imaging performance. To acquire accurate PSF, in this paper, we firstly scanned a phantom by SPW transmission, where only single scatterers were contained in the phantom. After that, PSF was obtained by fitting the generated SPW US image with 2-D Gaussian function. The fitting process was performed after aligning, normalizing, and averaging these microbubbles.

Fig. 4 further compares the localization accuracy obtained by the Gaussian fitting and CSRM methods, where more microbubbles overlapped. Fig. 4(a) shows the simulated US image from SPW transmission, where 10 microbubbles were randomly distributed in the phantom. Note that some of these microbubbles overlapped. Figs. 4(c) and (d) show the SR-US results obtained by Gaussian fitting and CSRM methods, respectively. As expect, when the microbubbles overlapped, they cannot be effectively identified by the Gaussian fitting method (see Fig. 4(c)). On the contrary, when using the proposed CSRM method, all microbubbles can be resolved (see Fig. 4(d)).

Table II quantitatively compares the localization errors of SR-US implemented by the proposed CSRM-SPW

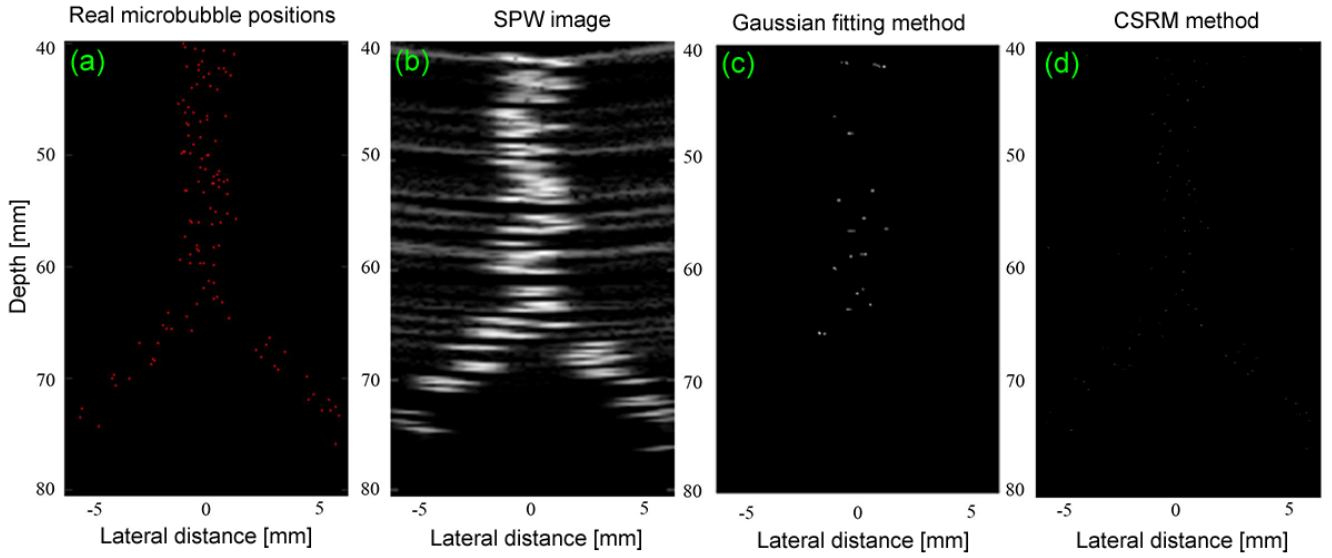

FIGURE 6. The simulated vasculature image from SPW imaging and its corresponding SR-US results, shown in the first frame. (a) The true positions of microbubbles in the vascular network model in the first frame. (b) The simulated vasculature image from SPW, shown in the first frame. (c) The corresponding SR-US result obtained by the Gaussian fitting method. (d) The corresponding SR-US result obtained by the proposed CSRM method.

TABLE 2. The localization errors of SR-US obtained by the proposed CSRM-SPW technique, incorporating the measurement data with varying SNRs.

Imaging modality \ SNR (dB)	10	20	30	40	50
SPW	0.17 mm	0.16 mm	0.16 mm	0.16 mm	0.16 mm

technique, incorporating the measurement data with varying SNRs (10, 20, 30, 40, and 50 dB). In this work, Cartesian distance between the reconstructed microbubble position and the nearest true microbubble position is used to measure the localization error. Note that SR-US image obtained by the CSRM method is a pixelated image representing the intensities of microbubbles, rather than a list of microbubble position coordinates. To calculate the localization error, it was necessary to convert the reconstructed SR-US image into a list of coordinates.

The quantitative results show that when using the CSRM-SPW technique, the localization error of SR-US is similar, whether the low or high noises are added to SPW images. The performance is important for the CSRM-SPW technique in real bio-medical application.

B. EVALUATING THE EFFECT OF STA AND SPW ON THE IMAGING PERFORMANCE OF SR-US OBTAINED BY THE CSRM METHOD

Fig. 5 demonstrates the effect of STA and SPW on the imaging performance of SR-US implemented by the CSRM method. Figs. 5(a) and (d) show the synthetic US images obtained from STA and SPW, respectively. Fig. 5(c) shows the SR-US image obtained by using the synthetic STA as the input data of the CSRM method. For comparison, Fig. 5(f) shows the SR-US image obtained by using the synthetic SPW as the input data of the CSRM method.

TABLE 3. The comparison of localization errors of SR-US obtained by using SPW and STA images as the input data of the CSRM method. Here, the synthetic SPW and STA data (i.e., the input data of the CSRM method) contains the different levels of noise.

Imaging modality \ SNR (dB)	10	20	30	40	50
STA	0.09 mm	0.09 mm	0.09 mm	0.09 mm	0.09 mm
SPW	0.09 mm	0.09 mm	0.09 mm	0.09 mm	0.09 mm

Table III further quantitatively compares the localization errors of SR-US implemented by using SPW and STA images as the input data of the CSRM method. To simulate the real application, the different levels of noise (SNR 10, 20, 30, 40, and 50 dB) were added to the synthetic US images.

The results show that when using the CSRM method, the obtained imaging performance of SR-US is similar, whatever STA or SPW images are used to reconstruct the super-resolution results. The quantitative results from Table III further confirm the conclusion. In another words, even if the low-spatial resolution US data (e.g., SPW US image) is used as the input data of the CSRM method, the localization accuracy of SR-US is not significantly affected. This means that by using SPW transmission combined with CSRM method (i.e., the proposed CSRM-SPW technique), we not only can obtain the high quality SR-US image, but also can speed up the imaging time of SR-US because of the use of SPW.

C. SUPER-RESOLUTION IMAGING OF MICROBUBBLES FLOWING IN VASCULAR NETWORK BY THE CSRM-SPW TECHNIQUE

Fig. 6 compares the performance of the CSRM and Gaussian fitting methods in resolving vascular network. Fig. 6(b) depicts the synthetic SPW image from the bubble-filled vascular network model, shown in the first frame. Fig. 6(c) shows the SR-US result obtained by the Gaussian fitting method. Fig. 6(d) shows SR-US result obtained by the CSRM method. Note that for Fig. 6(c) and Fig. 6(d), the synthetic SPW image (Fig. 6(b)) was used as the input data of the two methods. The results show that some overlapped microbubbles are not accurately identified by the Gaussian fitting method, which is similar with the results shown in Case I (see Fig. 3(c)). Comparably, when using the CSRM method, the most positions of microbubbles in vascular network can be effectively identified (see Fig. 6(d)).

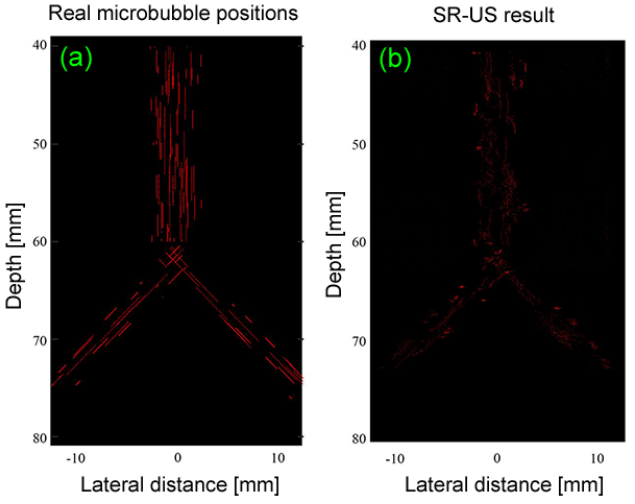

FIGURE 7. The SR-US result of the vasculature model implemented by the proposed CSRM method combined with SPW transmission technique. (a) The true positions of microbubbles in all 50 frame. (b) The SR-US result obtained by the proposed CSRM-SPW technique.

Finally, Fig. 7 demonstrates the ability of the proposed CSRM-SPW technique in resolving vascular network. Fig. 7(a) shows the true positions of microbubbles in all US frames (total in 50 frames). Fig. 7(b) shows the final SR-US result of the vascular network phantom model. Here, The SR-US result is obtained by applying the CSRM method to each SPW image. After determining the positions of the microbubbles in each frame, by superimposing the positions from all frames into an image, the final SR-US image is generated.

The results show that the vascular network can be resolved by the proposed CSRM-SPW technique. On the other hand, it should also note that because: 1) the highly overlapped microbubbles in each frame can be identified by the CSRM method; 2) the use of SPW transmission can further speed up the data acquisition of SR-US, the proposed CSRM-SPW (the CSRM method combined with SPW transmission) technique provides the potential in fast SR-US imaging study.

V. DISCUSSION AND CONCLUSION

US imaging is a widely used clinical imaging modality. However, the spatial resolution of traditional US imaging is limited to approximately half-wavelength. To improve the spatial resolution of US, recently, the super-resolution ultrasound (SR-US) technique has been proposed. SR-US breaks the diffraction limit and greatly improves the spatial resolution of US, which is important for the medical diagnosis and treatment. However, the temporal resolution of SR-US is still limited. To address the problem, in this paper, the compressed sensing reconstruction method combined with SPW transmission technique were used for implementing fast SR-US imaging. Especially, considering that SPW has a relative low spatial resolution due to the use of unfocused beams, it may affect the obtained SR-US imaging performance. To clarify the problem, in this paper, we study the effect of STA and SPW on the imaging performance of SR-US.

Based on the SR-US results from Case I, we can find that the overlapped microbubbles in the phantom model were not effectively identified by the conventional localization method (e.g., the Gaussian fitting method). On the contrary, when using the proposed CSRM method, the positions of all microbubbles can be effectively resolved, even if they overlapped (see Fig. 3, Fig. 4, and Table II). This means that by using the CSRM method, the imaging time of SR-US can be reduced because the number of frames used to implement SR-US imaging is greatly reduced. On the other hand, it can also be seen that when using the CSRM method, the obtained imaging performance of SR-US is similar, whatever using STA (high-resolution US image) or SPW (low-resolution US image) as the input data of the reconstruction method (see Fig. 5). The quantitative results from Table III further confirm the conclusion. This means that by using SPW transmission, the localization accuracy of SR-US obtained by the CSRM method is not significantly affected. But, the data acquisition time of SR-US can be further improved because of the use of SPW. Hence, the CSRM-SPW technique is suitable for fast SR-US imaging. The results from the flowing vasculature model further confirm the conclusion and validate the capability of the CSRM-SPW technique in imaging microbubbles flowing through vascular network (see Figs. 6 and 7). Based on the above results, we believe that the CSRM-SPW technique is suited for fast SR-US imaging.

However, in this paper, the numerical simulations were performed to validate the feasibility of CSRM-SPW method, which is simpler than real experimental study. In addition, in this work, the reconstruction method based on CS will greatly affect the SR-US imaging. The imaging performance of SR-US may be further improved by using or developing more efficient reconstruction methods [16]–[19]. On other hand, the matrix $\mathbf{A}$ shown in Eq. (1) is a key factor for SR-US imaging. Compared to super-resolution optical imaging,

in ultrasound imaging, some factors (e.g., the characteristics of coherent imaging, the background reflecting structures, and the point spread function, etc) may affect the construct of **A**. As a result, this may further affect the obtained SR-US imaging performance. In the future, we will carry out the systematic work on these problems.

In conclusion, by using the proposed CSRM-SPW technique, we can implement fast SR-US imaging. In future, we will apply the CSRM-SPW technique to perform fast SR-US imaging based on the physical phantom and animal experiments.

ACKNOWLEDGMENT

Yuexia Shu and Changpeng Han contribute equally to this paper.

REFERENCES

[1] P. R. Hoskins, K. Martin, and A. Thrush, Eds., *Diagnostic Ultrasound: Physics and Equipment*. Cambridge, U.K.: Cambridge Univ. Press, 2010.

[2] M. J. Rust, M. Bates, and X. Zhuang, "Sub-diffraction-limit imaging by stochastic optical reconstruction microscopy (STORM)," *Nature Methods*, vol. 3, no. 10, pp. 793–796, Aug. 2006.

[3] S. T. Hess, T. P. K. Girirajan, and M. D. Mason, "Ultra-high resolution imaging by fluorescence photoactivation localization microscopy," *Biophys. J.*, vol. 91, no. 11, pp. 4258–4272, Dec. 2006.

[4] O. M. Viessmann, R. J. Eckersley, K. Christensen-Jeffries, M. Tang, and C. Dunsby, "Acoustic super-resolution with ultrasound and microbubbles," *Phys. Med. Biol.*, vol. 58, no. 18, p. 6447, Sep. 2013.

[5] Y. Desailly, O. Couture, M. Fink, and M. Tanter, "Sono-activated ultrasound localization microscopy," *Appl. Phys. Lett.*, vol. 103, no. 17, p. 174107, 2013.

[6] C. Errico *et al.*, "Ultrafast ultrasound localization microscopy for deep super-resolution vascular imaging," *Nature*, vol. 527, no. 7579, pp. 499–502, Nov. 2015.

[7] A. Bar-Zion, C. Tremblay-Darveau, O. Solomon, D. Adam, and Y. C. Eldar, "Fast vascular ultrasound imaging with enhanced spatial resolution and background rejection," *IEEE Trans. Med. Imag.*, vol. 36, no. 1, pp. 169–180, Jan. 2017.

[8] Y. Shu, M. Lv, Y. Liu, Z. Yan, J. Jiang, and X. Liu, "Super-resolution ultrasound imaging with Gaussian fitting method and plane wave transmission," presented at the Conf. SPIE Med. Imag., Houston, TX, USA, 2018.

[9] M. Lv, Y. Shu, Y. Liu, Z. Yan, J. Jiang, and X. Liu, "A balanced super-resolution optical fluctuation imaging method for super-resolution ultrasound," presented at the Conf. SPIE Med. Imag., Houston, TX, USA, 2018.

[10] L. Zhu, W. Zhang, D. Elnatan, and B. Huang, "Faster STORM using compressed sensing," *Nature Methods*, vol. 9, pp. 721–723, Apr. 2012.

[11] H. P. Babcock, J. R. Moffitt, Y. Cao, and X. Zhuang, "Fast compressed sensing analysis for super-resolution imaging using L1-homotopy," *Opt. Exp.*, vol. 21, no. 23, pp. 28583–28596, 2013.

[12] L. Zhao *et al.*, "Improved imaging performance in super-resolution localization microscopy by YALL1 method," *IEEE Access*, vol. 6, pp. 5438–5446, 2018.

[13] O. Couture, S. Bannouf, G. Montaldo, J. F. Aubry, M. Fink, and M. Tanter, "Ultrafast imaging of ultrasound contrast agents," *Ultrasound Med. Biol.*, vol. 35, no. 11, pp. 1908–1916, 2009.

[14] M. Tanter and M. Fink, "Ultrafast imaging in biomedical ultrasound," *IEEE Trans. Ultrason., Ferroelectr., Freq. Control*, vol. 61, no. 1, pp. 102–119, Jan. 2014.

[15] J. A. Jensen, S. I. Nikolov, K. L. Gammelmark, and M. H. Pedersen, "Synthetic aperture ultrasound imaging," *Ultrasonics*, vol. 44, pp. e5–e15, Dec. 2006.

[16] I. Trots, A. Nowicki, and M. Lewandowski, "Synthetic transmit aperture in ultrasound imaging," *Arch. Acoust.*, vol. 34, no. 4, pp. 685–695, 2009.

[17] E. J. Candès and M. B. Wakin, "An introduction to compressive sampling," *IEEE Signal Process. Mag.*, vol. 25, no. 2, pp. 21–30, Mar. 2008.

[18] D. L. Donoho, Y. Tsaig, I. Drori, and J.-L. Starck, "Sparse solution of underdetermined systems of linear equations by stagewise orthogonal matching pursuit," *IEEE Trans. Inf. Theory*, vol. 58, no. 2, pp. 1094–1121, Feb. 2012.

[19] Q. Zhang, X. Chen, X. Qu, J. Liang, and J. Tian, "Comparative studies of ℓ_p-regularization-based reconstruction algorithms for bioluminescence tomography," *Biomed. Opt. Express*, vol. 3, no. 11, pp. 2916–2936, 2012.

[20] R. G. Baraniuk, V. Cevher, M. F. Duarte, and C. Hegde, "Model-based compressive sensing," *IEEE Trans. Inf. Theory*, vol. 56, no. 4, pp. 1982–2001, Apr. 2010.

[21] J. Yang and Y. Zhang, "Alternating direction algorithms for ℓ_1-problems in compressive sensing," *SIAM. J. Sci. Comput.*, vol. 33, no. 1, pp. 250–278, 2010.

[22] J. A. Jensen, "FIELD: A program for simulating ultrasound systems," *Med. Biol. Eng. Comput.*, vol. 4, no. 1, pp. 351–353, 1996.

[23] J. A. Jensen and N. B. Svendsen, "Calculation of pressure fields from arbitrarily shaped, apodized, and excited ultrasound transducers," *IEEE Trans. Ultrason., Ferroelectr., Freq. Control*, vol. 39, no. 2, pp. 262–267, Mar. 1992.

[24] M. C. Grant and S. P. Boyd. (2013). *CVX: MATLAB Software for Disciplined Convex Programming, Version 2.0 Beta*. [Online]. Available: http://cvxr.com/cvx

[25] J. Liu, Q. He, and J. Luo, "A compressed sensing strategy for synthetic transmit aperture ultrasound imaging," *IEEE Trans. Med. Imag.*, vol. 36, no. 4, pp. 878–891, Apr. 2017.

[26] J. Udesen, F. Gran, K. L. Hansen, J. A. Jensen, C. Thomsen, and M. B. Nielsen, "High frame-rate blood vector velocity imaging using plane waves: Simulations and preliminary experiments," *IEEE Trans. Ultrason., Ferroelectr., Freq. Control*, vol. 55, no. 8, pp. 1729–1743, Aug. 2008.

YUEXIA SHU received the bachelor's degree from the School of Electrical and Information Engineering, Jiangsu University, Zhenjiang, China, in 2016. She is currently pursuing the master's degree with the School of Communication and Information Engineering, Shanghai University, Shanghai, China. Her current research interests include super-resolution ultrasound imaging and x-ray luminescence/fluorescence computed tomography.

CHANGPENG HAN received the bachelor's and master's degrees from the Shanghai University of Traditional Chinese Medicine, Shanghai, China, where he is currently pursuing the Ph.D. degree. He is currently with the Yueyang Hospital of Integrated Traditional Chinese and Western Medicine, Shanghai University of Traditional Chinese Medicine. His current research interests include medical imaging, gastrointestinal tract and intestinal microbe, and surgery of gastrointestinal tract.

MINGLEI LV received the bachelor's degree from Zhejiang Sci-Tech University, Zhejiang, China, in 2012. He is currently pursuing the master's degree with the School of Communication and Information Engineering, Shanghai University. His current research interests include super-resolution fluorescence microscopy and ultrasound imaging.

XIN LIU (S'09–M'12) received the bachelor's and master's degrees from Fourth Military Medical University, Xian, China, in 2001 and 2006, respectively, and the Ph.D. degree (Hons.) in biomedical engineering from Tsinghua University, Beijing, China, in 2012. From 2001 to 2014, he was an Assistant Professor with the Department of Biomedical Engineering, Fourth Military Medical University. He is currently with the School of Communication and Information Engineering, Shanghai University, Shanghai, China. His publication record includes 30 papers, of which 16 are first-authored. He has also co-authored two book chapters. His current research interests include fluorescence molecular tomography, super-resolution fluorescence microscopy, and x-ray luminescence/fluorescence computed tomography.